FULL PAPER

H-Doped Black Titania with Very High Solar Absorption and Excellent Photocatalysis Enhanced by Localized Surface Plasmon Resonance

Zhou Wang, Chongyin Yang, Tianquan Lin, Hao Yin, Ping Chen, Dongyun Wan, Fangfang Xu,* Fuqiang Huang,* Jianhua Lin, Xiaoming Xie, and Mianheng Jiang

Black TiO_2 attracts enormous attention due to its large solar absorption and induced excellent photocatalytic activity. Herein, a new approach assisted by hydrogen plasma to synthesize unique H-doped black titania with a core/shell structure ($TiO_2@TiO_{2-x}H_x$) is presented, superior to the high H_2-pressure process (under 20 bar for five days). The black titania possesses the largest solar absorption (≈83%), far more than any other reported black titania (the record (high-pressure): ≈30%). H doping is favorable to eliminate the recombination centers of light-induced electrons and holes. High absorption and low recombination ensure the excellent photocatalytic activity for the black titania in the photo-oxidation of organic molecules in water and the production of hydrogen. The H-doped amorphous shell is proposed to play the same role as Ag or Pt loading on TiO_2 nanocrystals, which induces the localized surface plasma resonance and black coloration. Photocatalytic water splitting and cleaning using $TiO_{2-x}H_x$ is believed to have a bright future for sustainable energy sources and cleaning environment.

1. Introduction

Searching for efficient semiconductor photocatalysts utilizing visible-light solar energy for hydrogen generation from water splitting remains a great challenge.[1–5] Many efforts have been focused on enhancing visible light absorption by narrowing the band gap of TiO_2, including element doping and oxygen deficiency, but their visible-light absorption and power conversion still remain insufficient.[2,6–10] Recently, black titania with a narrow band gap (≈1.54 eV) was reported prepared from hydrogenating TiO_2 nanocrystals at 20 bar H_2 atmosphere for ≈5 days (HP–TiO_2), and its photocatalysis was greatly enhanced.[1] Since then, the synthesis of black titania has attracted plenty of attention.[11–16] The typical preparation method is to thermally anneal different titania precursors at ≈500 °C under a H_2 flow, but their photocatalytic activity was unsatisfied compared with pristine nanocrystals TiO_2.

Many theoretical models were employed to explain the black coloration of titania, which include surface disorder,[1] oxygen vacancy (Ti^{3+}),[11,15,16] and surface hydrogenation.[17,18] But these models are unable to perfectly uncover the bandgap narrowing and promise photocatalytic improvement. For example, the surface disorder of TiO_2 destroys lattice periodicity and the t_{2g} and e_g degeneracies of TiO_6 octahedra, generating two tails from the valence band maximum (VBM) and conduction band minimum (CBM) to narrow the band gap (E_g), but it is still insufficient to result in such a low E_g (1.54 eV) and the black coloration.[1] The amorphous TiO_2 without lattice ordering was reported to be white.[19] Apparently, other than developing a facile synthesis of black titania, more careful inspection is also demanded in explaining the mechanism.

It is well-known to produce TiH_2 foam by annealing Ti metal in the H_2 atmosphere at 400 °C,[20] and the small H atoms are active enough to incorporate in the lattice with elemental Ti. Herein, we report a new approach assisted by hydrogen plasma to produce black titania with a crystalline core/amorphous shell structure ($TiO_2@TiO_{2-x}H_x$). This black titania reveals very strong visible and infrared light absorption, which is believed to be induced by the localized surface plasmon resonance (LSPR). The LSPR is correlated with high carrier concentration of the amorphous shell. We elucidate the inner workings of the black $TiO_2@TiO_{2-x}H_x$ that has yielded over an order of magnitude improvement in the effectiveness of solar-driven photocatalysis.

Dr. Z. Wang, Dr. C. Yang, Dr. T. Lin, Dr. H. Yin,
Dr. P. Chen, Dr. D. Wan, Prof. F. Xu, Prof. F. Huang
CAS Key Laboratory of Materials for Energy Conversion
Shanghai Institute of Ceramics
Chinese Academy of Sciences
Shanghai, 200050, China
E-mail: ffxu@mail.sic.ac.cn; huangfq@mail.sic.ac.cn
Prof. F. Huang, Prof. J. Lin
Beijing National Laboratory for Molecular Sciences
and State Key Laboratory of Rare Earth Materials Chemistry
and Applications
College of Chemistry and Molecular Engineering
Peking University
Beijing 100871, China
Prof. X. Xie, Prof. M. Jiang
State Key Laboratory of Functional Materials for Informatics
Shanghai Institute of Microsystem and Information Technology
Chinese Academy of Sciences, Shanghai 200050, China

www.MaterialsViews.com

ADVANCED
FUNCTIONAL
MATERIALS
www.afm-journal.de

FULL PAPER
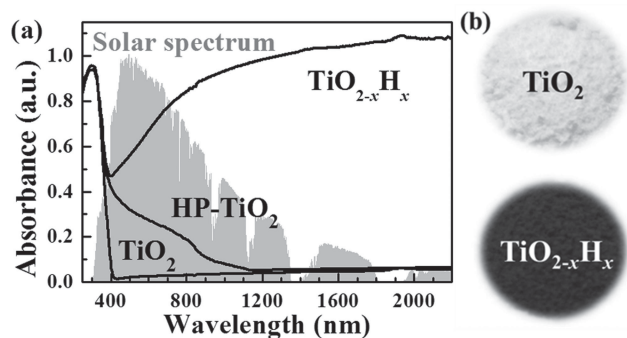
Figure 1. a) Diffuse reflectance spectra of our 8h-H-plasma-reduced black titania ($TiO_{2-x}H_x$), the high-pressure hydrogenated black titania (HP–TiO_2)[1], and pristine TiO_2 (P25, starting material). The background is the total solar spectrum. b) Photographs of black titania ($TiO_{2-x}H_x$) and pristine TiO_2.

2. Results and Discussion

Figure 1 displays the diffuse reflectance spectra of our 8h-H-plasma-reduced black titania (denoted as $TiO_{2-x}H_x$ in this context), the high-pressure hydrogenated black titania (HP-TiO_2) from the previous report,[1] and pristine TiO_2 nanocrystals (Degussa P25), where pristine TiO_2 and HP–TiO_2 are two references for comparison. For all samples, a steep increase in absorption at wavelengths shorter than ≈400 nm can be attributed to the intrinsic bandgap absorption of crystalline anatase TiO_2. Compared with P25, both $TiO_{2-x}H_x$ and HP–TiO_2 possess a significant absorption in the visible and near infrared light. Especially for the $TiO_{2-x}H_x$ sample, the visible and infrared light absorption drastically and monotonously increases at wavelengths longer than ≈400 nm, much superior to HP–TiO_2 and the other reported samples.[11–15] As shown in **Table 1**, The black titania possesses the extremely high solar absorption (83%), far more than HP–TiO_2 (≈30%). The enhanced light absorption in HP–TiO_2 was proposed to be due to introducing disorder in the surface layers of nanophase TiO_2 through hydrogenation and resulting in a secondary narrow bandgap (1.54 eV).[1] However, the absorption spectrum curve of HP–TiO_2 is very similar to the reported results for TiO_2 crystals modified by noble metal (Ag, Pt, Au) nanoparticles.[21–24] The enhanced visible light absorption in Ag-loaded TiO_2 samples is assigned to the LSPR, and a similar secondary "bandgap" ranges from 1.75 to 2.75 eV.[25] Large wide-spectrum absorption for $TiO_{2-x}H_x$ sample is analogous to the Pt-loaded TiO_2 samples due to the LSPR, which does not have a similar secondary bandgap.[22] All these noble metal-loaded TiO_2 have a similar

black or grey color and the black coloration mainly depends on the adding the amount of noble metal,[22] consistent with not only the reported results[21–24] but also our prepared Ag-TiO_2 samples (Figure S1, Supporting Information).

For Ag or Pt-loaded TiO_2, the enhanced visible-light absorption peak is due to that the incident photon frequency is resonant with the collective excitations of the conduction electrons of noble-metal nanoparticles,[26,27] which may also happen in our and the reported black titania samples. The treatment of hydrogen plasma or high-pressure hydrogen gas could convert surfaced Ti^{4+} ($3d^0$) into Ti^{3+} ($3d^1$) by introducing H doping ($TiO_{2-x}H_x$) or/and oxygen vacancies (TiO_{2-x-x}), which both increase carrier (electron) concentration. Generally, the LSPR effect is closely related to surface carrier concentration. The concentration of charge carriers and the large photon absorption induced by LSPR effect should change simultaneously with the amount of Ti–H bonds and Ti^{3+}. In order to prove it, the $TiO_{2-x}H_x$ samples with different hydrogenation time were investigated. As shown in Figure S2 and Table S1, Supporting Information, the light absorbance and carrier concentration of the $TiO_{2-x}H_x$ samples show an increasing trend, which is consistent with the LSPR effect. The $TiO_{2-x}H_x$ samples were further treated in 50 °C-stirring H_2O_2 solution to oxidize the hydrogenated state while preserving the surface amorphous structure. The carrier concentration falls to a degree lower than the hall measurement limit, and the absorbance sharply decreases without a raised peak in visible and infrared-light region. We also investigated the electron transport behavior of black titania films. Two anatase TiO_2 films prepared by magnetron sputtering (thickness: 223 nm, 663 nm) were treated by the same hydrogen plasma process. Interestingly, the n-type films obtained not only enhanced visible and infrared light absorption (Figure S3, Supporting Information) but also a rather high electron concentration (7.3×10^{20} cm^{-3}, 7.8×10^{20} cm^{-3}) resulting in a low sheet resistance (98.3 Ω sq^{-1}, 69.6 Ω sq^{-1}). Conduction electrons with such high concentration in black titania are enough to cause the LSPR, therefore it is not surprising that the enhanced absorption of our black titania was observed after hydrogen plasma treatment. Similar phenomenon also happens in transparent conducting oxide (TCO) films. The TCO film has a large absorption in the near infrared light range when the electron concentration is high (>10^{20} cm^{-3}).[28]

Hydrogen plasma process offers high-energy species such as electrons, atoms, and radicals, which improves thermodynamics and kinetics over conventional processing.[29,30] It is the key why our well-crystallized sample is much easier be converted in deep black than the H_2-annealing sample (light grey, see the comparison in Figure S4, Supporting Information). In order to uncover the microstructure, the black $TiO_{2-x}H_x$ sample was examined by the high resolution transmission electron microscopy (HRTEM), as shown in **Figure 2**a. The black $TiO_{2-x}H_x$ nanoparticles have a hydrogen-stabilized amorphous layer surrounding a crystalline core to form an amorphous shell/crystalline core structure ($TiO_2@TiO_{2-x}H_x$), compared with highly-crystallized pristine TiO_2 with clear lattice fringes shown in Figure 2b. The size of individual nanoparticles is approximately 20 nm in diameter. The disordered surface layer with ≈2 nm in thickness is coated on a crystalline core after the hydrogen plasma process for 8 h. The structural changes
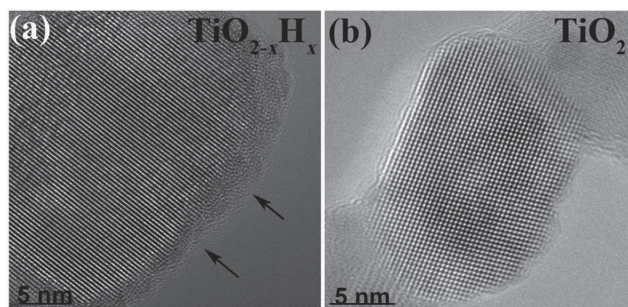
Table 1. Solar absorption in different spectrum region.

Sample	total	UV[a]	Visible[b]	Infrared[c]
solar spectrum	100%	7%	50%	43%
pristine TiO_2	5%	5%	0	0
$TiO_{2-x}H_x$	83%	6%	39%	38%
HP–TiO_2	30%	5%	24%	1%

[a]UV light: <400 nm; [b]visible light: 400–760 nm; [c]infrared light: >760 nm.

FULL PAPER

Figure 2. HRTEM images of a) black $TiO_{2-x}H_x$ and b) pristine TiO_2.

were further examined by measuring Raman scattering of the $TiO_{2-x}H_x$ sample (Figure S5, Supporting Information). For pristine TiO_2, there are six Raman active modes ($3E_g + 2B_{1g} + A_{1g}$) with frequencies at 144, 197, 399, 515, 519 (superimposed with the 515 cm^{-1} band), and 639 cm^{-1}, respectively.[31] The shifting and broadening of the $TiO_{2-x}H_x$ Raman peaks indicate that the original symmetry of TiO_2 lattice is broken down due to the disorder surface after hydrogen plasma process.

The black coloration of TiO_2 cannot bypass to check the existence of Ti^{3+}. The plots in **Figure 3** show the electron paramagnetic resonance (EPR) and magnetic measurements of pristine TiO_2, $TiO_{2-x}H_x$, and oxygen deficient titania (TiO_{2-x}), which are widely-used to examine unpaired spins and magnetism. The TiO_{2-x} sample shows very strong response from Ti^{3+} spins and a superparamagnetic behavior due to localized Ti^{3+} $3d^1$ states, consistent with the previous study.[32] Pristine TiO_2 and $TiO_{2-x}H_x$ only possess a very weak form of resonance at g-value of 2.02 which results from surface adsorbed O_2^- from air.[33] The absence of EPR signal at about $g = 1.957$, which is characteristic of paramagnetic Ti^{3+} centers, indicates the absence of the Ti^{3+} spins in the $TiO_{2-x}H_x$ (Figure 3a). The very weak paramagnetism (<0.04 emu g^{-1}) existing in both $TiO_{2-x}H_x$ and pristine TiO_2 samples further confirms the absence of the Ti^{3+} spins (Figure 3b). Localized Ti^{3+} states/oxygen vacancies are considered to promote the recombination of light-excited electrons and holes, and to be one of the originations of photoluminescence.[34] However, these two types of measurements cannot exclude the existence of Ti^{3+} in the $TiO_{2-x}H_x$. Similarly, the phase of Ti_2O_3 contains no localized moments on the Ti^{3+} ions, which are confirmed by neutron polarization studies,[35] although the oxidation state of Ti is +3.

X-ray photoelectron spectroscopy (XPS) is a powerful tool to investigate the change of surface chemical bonding as well as the electronic valence band position, as shown in **Figure 4**. The Ti 2p XPS spectra were almost identical for pristine TiO_2 and $TiO_{2-x}H_x$ with Ti $2p_{3/2}$ and $2p_{1/2}$ peaks centered at binding energies of 458.5 and 464.3 eV, which are typical for the Ti^{4+}–O bonds in TiO_2.[36] The hydrogen plasma introduces an additional broad peak centered at 457.1 eV, which is attributed to the surface Ti–H bonds.[16] The O 1s XPS spectra of two samples only show small differences (Figure 4b). The single O 1s peak at 529.8 eV in pristine TiO_2 is typically assigned to Ti–O bonds. The slightly broader O 1s peak in $TiO_{2-x}H_x$ is due to a small peak at about 531.8 eV from Ti–OH bonds, much smaller than the reported results.[11] Both valence band spectra
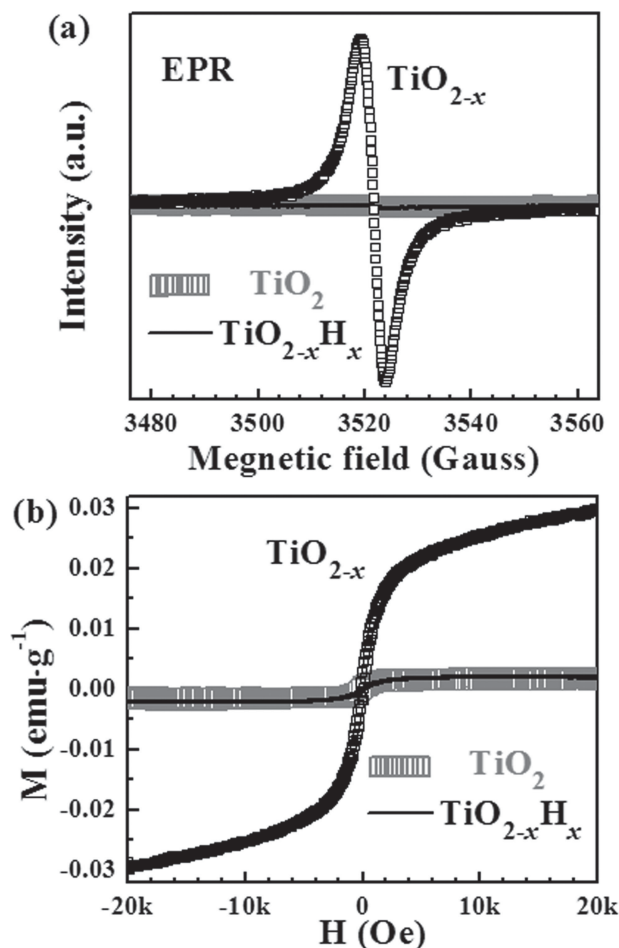

Figure 3. a) EPR spectra and b) magnetic measurements of $TiO_{2-x}H_x$, TiO_2, and TiO_{2-x}.

in Figure 4c are also similar, consistent with the reported H_2-annealed TiO_2.[11] The valence band maxima are estimated by linear extrapolation of the peaks to the baselines, which derives a band edge position of 2.05 eV below the Fermi energy for the both samples, which is close to the reported value.[37] The hydrogen plasma treatment has a negligible effect on valence band position of the TiO_2 surface.

The photoluminescence (PL) emission spectra may be useful to understand the behavior of light-generated electrons and holes in our samples since PL emission results from the recombination of free carriers.[38,39] The PL spectra of pristine and hydrogenated TiO_2 samples in the wavelength range of 350–700 nm with the excitation at 320 nm are shown in Figure 4d. Their emission spectra shapes are very similar. Three main emission peaks are located at about 403 nm (3.1 eV), 423 nm (2.9 eV), and 464 nm (2.7 eV), respectively. The first one is attributed to the emission of bandgap transition corresponding to the bandgap energy of anatase. The peaks at 450 nm and 468 nm are attributed to band edge free excitons. The other two peaks at 482 nm and 492 nm are due to bound excitons.[39] In addition, some small PL peaks observed in the wavelength
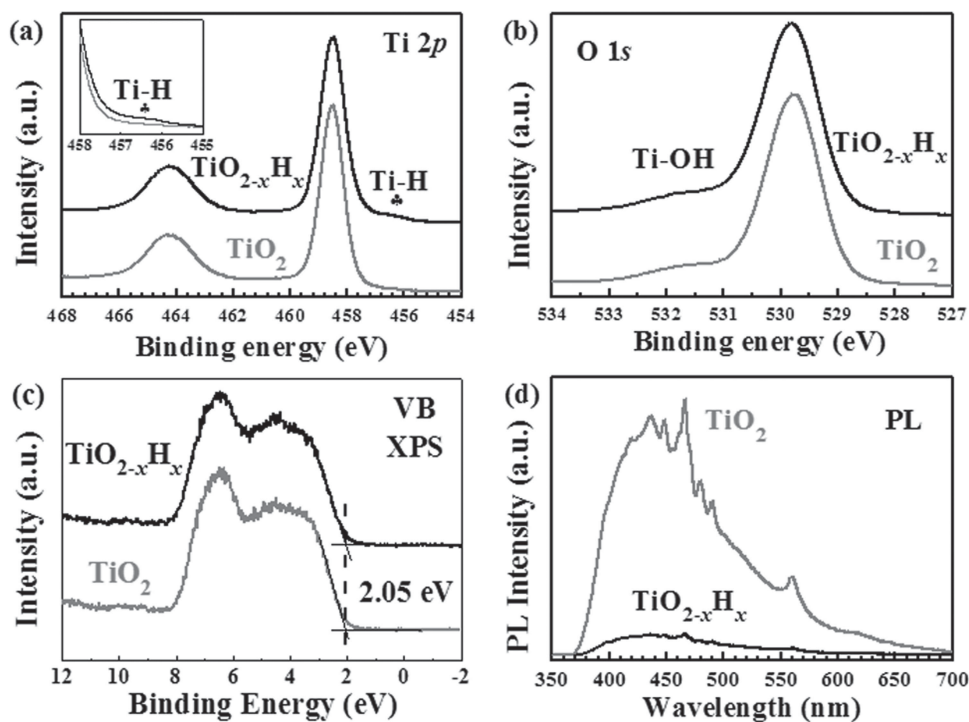
Figure 4. Pristine TiO_2 and black $TiO_{2-x}H_x$: a) Ti 2p XPS spectra, b) normalized O 1s XPS spectra, c) XPS valence band spectra, and d) photoluminescent spectra.

may mainly result from surface defects of the TiO_2 samples. The PL peak intensity of the black $TiO_{2-x}H_x$ sample reveals a significant decrease compared with pristine TiO_2. The PL intensity of $TiO_{2-x}H_x$ decreases with increasing the treatment time of hydrogen plasma (Figure S6, Supporting Information). Similar PL decreasing was also found in the samples of Ag or Pt-loaded TiO_2, which is due to the LSPR.[40] All the results indicate that the $TiO_{2-x}H_x$ sample has a relative low recombination rate of electrons and holes. Normally, low recombination rate of electrons and holes favors high photocatalytic activity.
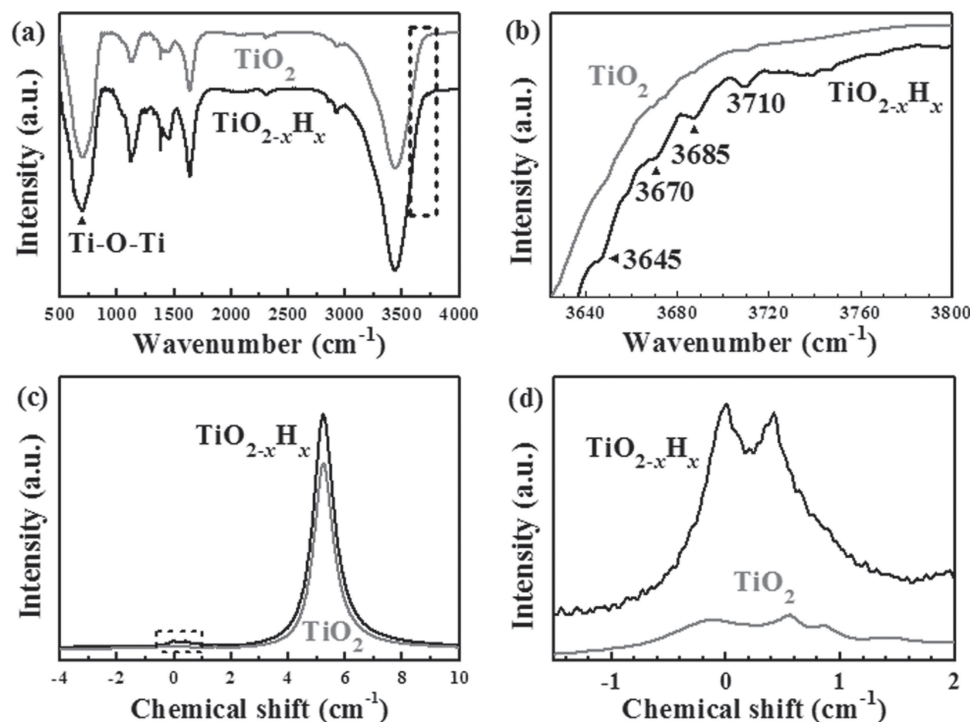
To gain further insights on chemical changes caused by the hydrogenation, Fourier transform infrared (FTIR) spectroscopic measurements were performed, as shown in **Figure 5**a,b. A characteristic feature of the spectrum is the presence of a band at ≈710 cm^{-1} due to symmetric stretching vibrations of the Ti–O bonds of the TiO_4 tetrahedra.[41] Both materials seem to show similar absorption features from 500 cm^{-1} to 4000 cm^{-1}, and both exhibit OH absorption bands near the 1635 cm^{-1} and 3400 cm^{-1} region. The difference of spectrum (Figure 5b) reveals that hydrogenation leads to additional absorption peaks at 3645, 3670, and 3685 cm^{-1}, which are characteristic of tetrahedral coordinated vacancies, and designated Ti^{4+}–OH, in accordance with previous results for hydroxylated titania.[42] Moreover, hydrogenation leads to another new absorbance at 3710 cm^{-1}, corresponding to terminal OH groups, which could be attributed to the hydrogen atoms embedded in the TiO_2 network.[43]

^1H NMR measurements were conducted to further examine the role of hydrogenation in black TiO_2, as shown in Figure 5c,d. Both the black and white TiO_2 show a large peak at
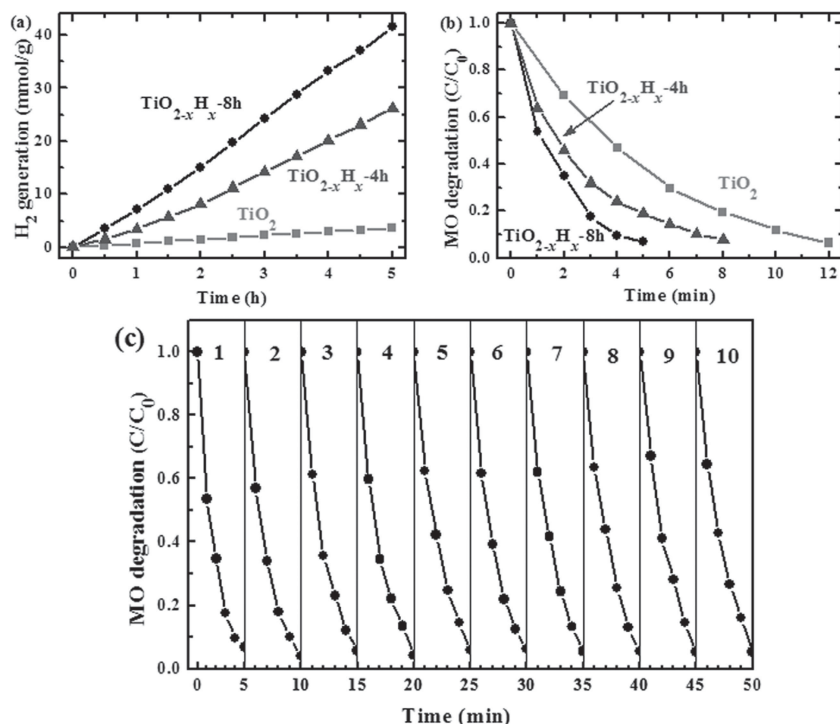
chemical shift of 5.5 ppm. The slightly larger linewidth in black TiO_2 may be caused by the incorporation of H at bridging sites at the disordered phase produced during the hydrogenation process, or may be due to the bridging sites located on different crystallographic planes on the surface.[44] Additionally, the stronger peak at 5.5 ppm suggests stronger hydrogen-bonded bridging hydroxyl groups in the black TiO_2. In contrast to pristine white TiO_2, black $TiO_{2-x}H_x$ shows that two additional sharp resonances at chemical shifts of 0.4 ppm and 0.01 ppm are observed on top of a broad base. The additional signals at δ = 0.4 and 0.01 ppm can be assigned to the terminal and internal hydroxyl groups of anatase, respectively, which are associated with hydrogen located in the disordered surface layer of the black TiO_2 as a result of hydrogenation.[45]

Over all, the black coloration of TiO_2 may be due to possible defect states including H doping, oxygen vacancies and surface hydroxyl groups on TiO_2. Apparently, the oxygen vacancies in the amorphous shell are unstable in hydrogen plasma, which would be filled by small H atoms. H doping rather than oxygen vacancies is the origination of the itinerant electrons of Ti^{3+} $3d^1$ at the CBM, which is responsible for a rather high electron concentration. In other word, H doping in an amorphous shell enhanced light absorption and reduced the localized Ti^{3+} states (e–h recombination centers), which would be helpful to improve photocatalytic activity.

The photocatalytic activities (H_2 generation, water cleaning) of the $TiO_{2-x}H_x$ sample ($TiO_{2-x}H_x$-8h), which was prepared from pristine TiO_2 in a hydrogen plasma for 8 h at 500 °C, are illustrated in **Figure 6**. Under the solar light irradiation, the $TiO_{2-x}H_x$ steadily produced hydrogen gas up to 8.2 mmol h^{-1} g^{-1}

ADVANCED
FUNCTIONAL
MATERIALS
www.afm-journal.de

Materials
Views
www.MaterialsViews.com

FULL PAPER

Figure 5. a,b) FTIR and c,d) ^{1}H NMR spectra of pristine TiO_2 and $TiO_{2-x}H_x$.

Figure 6. a) Solar-light driven photocatalytic water splitting for H_2 generation and b) solar-light driven photocatalytic decomposition of methyl orange over pristine TiO_2, $TiO_{2-x}H_x$-4h, and $TiO_{2-x}H_x$-8h ($TiO_{2-x}H_x$). c) Cycling tests of solar-driven photocatalytic activity of $TiO_{2-x}H_x$-8h.

(Figure 6a), compared with pristine TiO_2 (0.61 mmol h^{-1} g^{-1}). Our $TiO_{2-x}H_x$ sample shows a noticeable improvement, which belongs to the best ranks (≈10 mmol h^{-1} g^{-1}) among the TiO_2-based photocatalysts measured under the similar conditions.[1] In order to evaluate the ability of degrading organic contaminants, methyl orange (MO) was used as a probe molecule. Shown in Figure 6b, the black $TiO_{2-x}H_x$ sample excellently completed the MO degradation in 5 min under in the irradiation of solar light, while the white pristine TiO_2 (P25) took 12 min. The hydrogen generation and MO degradation of the $TiO_{2-x}H_x$-4h sample are better than pristine TiO_2 but poorer than $TiO_{2-x}H_x$-8h ($TiO_{2-x}H_x$). The cycling tests reveal that the black $TiO_{2-x}H_x$ sample was very stable in ten photocatalysis cycles, as shown in Figure 6c. All these investigations demonstrate that our black titania promises improved photocatalytic activity. Hydrogen plasma process is proved to be an excellent method to prepare black titania with efficient photocatalysis.

In order to further understand our black titania, the energy band diagram scheme of the core/shell structure (TiO_2@$TiO_{2-x}H_x$) is schematized in **Figure 7**a. The amorphous shell of TiO_2 loses lattice periodicity and breaks the octahedral symmetry of TiO_6, and
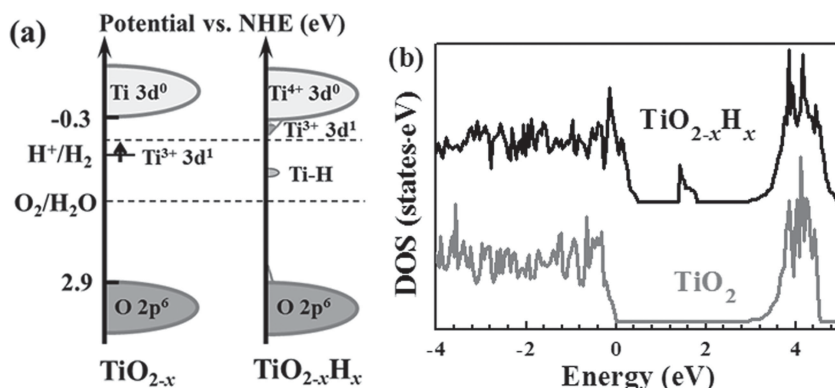
Figure 7. a) Proposed energy band diagram scheme of hydrogenated titania ($TiO_{2-x}H_y$) and oxygen deficiency TiO_{2-x}. b) Calculated DOS of pristine TiO_2 and black $TiO_{2-x}H_x$.

two tails of the VBM and CBM are formed which can narrow the band gap. But this is not sufficient to the black coloration of TiO_2; instead our amorphous TiO_2 sample has few E_g change, as shown in Figure S7, Supporting Information. It should be noted that the Ti–H bonds in the amorphous shell ($TiO_{2-x}H_x$) could form the intermediate states in the band gap. The electronic structures were calculated by first-principle theoretical calculations, and the computational details are in Supporting Information. The hydrogenation tends to produce shallow energy levels near the conduction band minimum and the midgap electronic states in the band gap. From the calculated total and projected DOS, we found that the primary effect of surface defects and reconstruction in TiO_2 nanocrystals is to produce strong band tailing near the conduction band edge. The tailing effect leads a remarkable bandgap narrowing (≈ 0.8 eV). Furthermore, H atoms introduce localized states at 0.92–1.37 eV below the CB minimum of black $TiO_{2-x}H_x$ (Figure 7b). Therefore, the electronic transitions from the tailed VB and midgap electronic states to CBM are responsible for the Vis–NIR absorption in our $TiO_{2-x}H_x$.

3. Conclusions

The core/shell structure $TiO_2@TiO_{2-x}H_x$ sample was prepared by hydrogen plasma method. The black titania possesses the largest solar absorption (83%) among the recently developed black titania. The enhanced solar light absorption of $TiO_{2-x}H_x$ is attributed to the amorphous shell, which is believed to induce the localized surface plasmon resonance similarly found in Ag or Pt-loaded TiO_2. Our hydrogen treatment can reduce the localized Ti^{3+} states, which is the recombination center of light-excited electrons and holes, and produce efficient photcatalyst. Photocatalytic water splitting and cleaning using $TiO_{2-x}H_x$ continue to be a dream for sustainable energy sources and cleaning environment.

4. Experimental Section

Preparation of Black $TiO_{2-x}H_x$: The hydrogenation of TiO_2 was performed in a thermal plasma furnace by hydrogen plasma for 4–8 h at 500 °C. The plasma input power was 200 W.

Preparation of Black TiO_{2-x}: The preparation of oxygen vacancy titania for comparison as described in earlier report.[46] A commercial amorphous TiO_2 was used as precursor. The amorphous powder (1.0 g) was initially heated at 200 °C under flowing O_2 for 1 h, in order to oxidize and favor the desorption of molecular species adsorbed onto the surface of the metal oxide. After cooled to room temperature, the obtained TiO_2 was reduced in H_2 flow at 500 °C for 1 h.

Photocatalytic Methyl Orange Decomposition: The photocatalytic activities of the TiO_2 samples were evaluated by monitoring the decomposition of methyl orange in an aqueous solution under solar light irradiation. After stirring for 30 min under UV light irradiation to stabilize the black TiO_2 in water, the black TiO_2 (100 mg) was filtered and mixed with methyl orange solution (100 mL, 0.1 M), which was subsequently illuminated with an AM 1.5 solar power system. The photocatalysis reaction was carried out at pH = 1.0.

Photocatalytic H_2 Generation: Photocatalyst (100 mg) loaded with Pt (0.5 wt.%) was placed into an aqueous methanol solution (120 mL, 25%) in a closed-gas circulation system. An AM 1.5 solar power system was used as light irradiation source. Methanol was used as a sacrificial reagent, and the anodic reaction generating O_2 from H_2O did not occur.

Sample Characterization: Raman spectra were collected on a Thermal Dispersive Spectrometer using a laser with an excitation wavelength of 532 nm at laser power of 10 mW. Solid-state ^1H magic-angle spinning (MAS) NMR spectra were acquired on a Bruker Ascend-400 spectrometer (400.3 MHz) using standard Bruker pulse programs, as well as a modified pulse program in order to incorporate dipolar dephasing into the direct ^{13}C pulse experiment. XPS experiments were carried out on a RBD upgraded PHI-5000C ESCA system (Perkin Elmer) with Mg Kα radiation ($h\nu$ = 1253.6 eV). FTIR spectra were recorded on Perkin-Elmer Spectrum 100 using KBr disks. The EPR spectra were collected using a Bruker EMX-8 spectrometer at 9.44 GHz at 300 K. The magnetic performance was conducted by a Physical Property Measurement System (PPMS, Quantum Design Company). XRD patterns were obtained with a Bruker D8 advance diffractometer operating with Cu Kα radiation.

Supporting Information

Supporting Information is available from the Wiley Online Library or from the author.

[1] X. Chen, L. Liu, P. Y. Yu, S. S. Mao, *Science* **2011**, *331*, 746–750.

[2] R. Asahi, T. Morikawa, T. Ohwaki, K. Aoki, Y. Taga, *Science* **2001**, *293*, 269–271.

[3] X. Lü, F. Huang, X. Mou, Y. Wang, F. Xu, *Adv. Mater.* **2010**, *22*, 3719–3722.

[4] X. Lü, X. Mou, J. Wu, D. Zhang, L. Zhang, F. Huang, F. Xu, S. Huang, *Adv. Funct. Mater.* **2010**, *20*, 509–515.

[5] Z. Zou, J. Ye, K. Sayama, H. Arakawa, *Nature* **2001**, *414*, 625–627.

[6] X. Chen, S. S. Mao, *Chem. Rev.* **2007**, *107*, 2891–2959.

[7] W. Choi, A. Termin, M. R. Hoffmann, *J. Phys. Chem.* **1994**, *98*, 13669–13679.

[8] J. H. Park, S. Kim, A. J. Bard, *Nano Lett.* **2005**, *6*, 24–28.

[9] T. Umebayashi, T. Yamaki, H. Itoh, K. Asai, *Appl. Phys. Lett.* **2002**, *81*, 454–456.

[10] J. Wang, D. N. Tafen, J. P. Lewis, Z. Hong, A. Manivannan, M. Zhi, M. Li, N. Wu, *J. Am. Chem. Soc.* **2009**, *131*, 12290–12297.

[11] G. Wang, H. Wang, Y. Ling, Y. Tang, X. Yang, R. C. Fitzmorris, C. Wang, J. Z. Zhang, Y. Li, *Nano Lett.* **2011**, *11*, 3026–3033.

[12] H. Pan, Y. W. Zhang, V. B. Shenoy, H. Gao, *J. Phys. Chem. C* **2011**, *115*, 12224–12231.

[13] S. Hoang, S. P. Berglund, N. T. Hahn, A. J. Bard, C. B. Mullins, *J. Am. Chem. Soc.* **2012**, *134*, 3659–3662.

[14] C. Sun, Y. Jia, X. H. Yang, H. G. Yang, X. Yao, G. Q. Lu, A. Selloni, S. C. Smith, *J. Phys. Chem. C* **2011**, *115*, 25590–25594.

[15] X. Jiang, Y. Zhang, J. Jiang, Y. Rong, Y. Wang, Y. Wu, C. Pan, *J Phys. Chem. C* **2012**, *116*, 22619–22624.

[16] Z. Zheng, B. Huang, J. Lu, Z. Wang, X. Qin, X. Zhang, Y. Dai, M. H. Whangbo, *Chem. Commun.* **2012**, *48*, 5733–5735.

[17] W. Wang, Y. R. Ni, C. H. Lu, Z. Z. Xu, *RSC Adv.* **2012**, *2*, 8286–8288.

[18] J. B. Lu, Y. Dai, H. Jin, B. B. Huang, *Phys. Chem. Chem. Phys.* **2011**, *13*, 18063–18068.

[19] A. Naldoni, M. Allieta, S. Santangelo, M. Marelli, F. Fabbri, S. Cappelli, C. L. Bianchi, R. Psaro, V. Dal Santo, *J. Am. Chem. Soc.* **2012**, *134*, 7600–7603.

[20] K. M. Mackay, *Hydrogen Compounds of the Metallic Elements*, E. and F. N. Spon, London, UK **1966**, 71.

[21] T. Hirakawa, P. V. Kamat, *J. Am. Chem. Soc.* **2005**, *127*, 3928–3934.

[22] J. Yu, L. Qi, M. Jaroniec, *J. Phys. Chem. C* **2010**, *114*, 13118–13125.

[23] Z. W. Seh, S. Liu, M. Low, S. Y. Zhang, Z. Liu, A. Mlayah, M. Y. Han, *Adv. Mater.* **2012**, *24*, 2310–2314.

[24] P. Wang, B. B. Huang, X. Y. Qin, X. Y. Zhang, Y. Dai, J. Y. Wei, M. H. Whangbo, *Angew. Chem. Int. Ed.* **2008**, *47*, 7931–7933.

[25] M. Hari, S. A. Joseph, S. Mathew, P. Radhakrishnan, V. P. N. Nampoori, *J. Appl. Phys.* **2012**, *112*, 074307.

[26] J. Yu, G. Dai, B. Huang, *J. Phys. Chem. C* **2009**, *113*, 16394–16401.

[27] J. Yu, H. Tao, B. Cheng, *ChemPhysChem* **2010**, *11*, 1617–1618.

[28] M. Grundmann, *The Physics of Semiconductors*, Vol. *19*: Springer Verlag, Berlin, Heidelberg, Germany **2010**, 511–515.

[29] D. Bullard, D. Lynch, *Metall. Mater. Trans. B* **1997**, *28*, 1069–1080.

[30] R. A. Palmer, T. M. Doan, P. G. Lloyd, B. L. Jarvis, N. U. Ahmed, *Plasma Chem. Plasma P.* **2002**, *22*, 335–350.

[31] X. Chen, S. S. Mao, *Chem. Rev.* **2007**, *107*, 2891–2959.

[32] J. Strunk, W. C. Vining, A. T. Bell, *J. Phys. Chem. C* **2010**, *114*, 16937–16945.

[33] S. M. Prokes, J. L. Gole, X. Chen, C. Burda, W. E. Carlos, *Adv. Funct. Mater.* **2005**, *15*, 161–167.

[34] X. Wang, Z. Feng, J. Shi, G. Jia, S. Shen, J. Zhou, C. Li, *Phys. Chem. Chem. Phys.* **2010**, *12*, 7083–7090.

[35] R. M. Moon, T. Riste, W. C. Koehler, S. C. Abrahams, *J. Appl. Phys.* **1969**, *40*, 1445–1447.

[36] M. S. Lazarus, T. K. Sham, *Chem. Phys. Lett.* **1982**, *92*, 670–674.

[37] J. Pan, G. Liu, G. Q. Lu, H. M. Cheng, *Angew. Chem. Int. Ed.* **2011**, *50*, 2133–2137.

[38] J. C. Yu, G. J. Yu, W. K. Ho, Z. T. Jiang, L. Z. Zhang, *Chem. Mater.* **2002**, *14*, 3808–3816.

[39] Q. Xiang, K. Lv, J. Yu, *Appl. Catal. B* **2010**, *96*, 557–564.

[40] B. Xin, L. Jing, Z. Ren, B. Wang, H. Fu, *J. Phys. Chem. B* **2005**, *109*, 2805–2809.

[41] V. A. Zeitler, C. A. Brown, *J. Phys. Chem.* **1957**, *61*, 1174–1177.

[42] P. M. Kumar, S. Badrinarayanan, M. Sastry, *Thin Solid Films* **2000**, *358*, 122–130.

[43] S. H. Szczepankiewicz, A. J. Colussi, M. R. Hoffmann, *J. Phys. Chem. B* **2000**, *104*, 9842–9850.

[44] P. Jonsen, *Colloids Surf.* **1989**, *36*, 127–132.

[45] M. Crocker, R. H. M. Herold, A. E. Wilson, M. Mackay, C. A. Emeis, A. M. Hoogendoorn, *J. Chem. Soc., Faraday Trans.* **1996**, *92*, 2791–2798.

[46] A. Naldoni, M. Allieta, S. Santangelo, M. Marelli, F. Fabbri, S. Cappelli, C. L. Bianchi, R. Psaro, V. Dal Santo, *J. Am. Chem. Soc.* **2012**, *134*, 7600–7603.